BIOCHEMISTRY

Reset-free DNA logic circuits for real-time input processing and memory

Junho Sim[1]†, Taehoon Kim[1]†, Woojin Kim[1]†, Sangeun Jeong[1], Eunjin Choi[1,2], Sion Kim[3], Hansol Choi[4], Sung Sun Yim[5,6], Yeongjae Choi[5]*

DNA logic circuits have great potential for biocompatible and programmable computations; however, current designs require reset processes, which restrict real-time data processing and memory functionality. This study proposes a reset-free approach on the basis of toehold-mediated chain reaction (TCR), which enables continuous and reversible strand migration within dual-rail units. By localizing TCR components on two-dimensional DNA origami templates, various combinational logic gates (e.g., AND and OR gates) and memory elements were implemented, including set-reset and data latches, as well as advanced cascaded registers. These circuits consistently processed new inputs and retained outputs over multiple sequential operations. The proposed reset-free TCR framework offers a mechanism most analogous to electronic circuit operation and demonstrates considerable potential for practical applications in biosensing, diagnostics, and synthetic biology.

INTRODUCTION

DNA logic circuits have been widely studied in fields such as computation (*1*–*5*), molecular diagnostics (*6*–*9*), programmable nanostructures (*10*–*16*), artificial neural networks (*17*–*19*), and DNA walkers (*20*–*22*) owing to their biocompatibility, DNA origami–based programmability, and inherent parallel processing capabilities. Current research is focused on developing fundamental components analogous to those used in conventional digital computing, with early demonstrations including combinations of basic logic operations, such as four-bit square-root circuits and full adders (*23*–*25*).

Despite these achievements, most DNA logic circuits require a reset step to accept new inputs, which limits their ability to handle real-time inputs and implement complex memory-based circuits (*26*). DNA logic gates operating via toehold-mediated strand displacement (TMSD) reactions typically undergo structural changes upon activation, which prevent further inputs from being accepted without an additional resetting procedure (*27*–*30*). TMSD-based logic gates function by exchanging an output strand with an input strand (*31*, *32*). The input strand interacts with the substrate-output complex through its toehold domain, which initiates branch migration and displaces the output strand. Subsequently, the output strand departs, and the input strand forms a stable complex with the substrate, which prohibits reverse reactions and further input processing. These limitations can be overcome by adding a secondary toehold domain to the strands (*33*–*35*). This additional toehold enables the separation of past input strands and the restoration of the output strands, thereby allowing a TMSD-based reset. However, this reset process markedly increases the design complexity and limits scalability, particularly when inputs change continuously or gates are cascaded. Cascaded gate arrangements require a TMSD-based reset across all the gate elements, which complicates circuit reuse and limits its real-time input processing. Moreover, given that circuit operation inherently requires a reset step, memory implementation remains unfeasible. Thus far, efforts to eliminate the reset step in DNA logic circuits have been limited to a few types of single gates, and comprehensive design guidelines for complex systems are lacking (*33*, *35*).

In this study, we used toehold chain reactions (TCRs) as a core mechanism for reset-free DNA logic circuits that can continuously accept new inputs (Fig. 1A). TCR uses DNA signal strands with binding affinities comparable to those of the DNA gate strands. In the TCR system, signal strands propagate to subsequent gates through cascading toehold exchange, analogous to carrier flow in electronic circuits, which causes them to become aligned. To ensure reaction fidelity, TCR components are spatially localized on a DNA origami template, thereby minimizing undesired interactions between nonadjacent strands (Fig. 1B). The alignment direction is determined on the basis of the initial input provided to the overall circuit. Two signal components with identical toehold lengths and comparable GC content compete to bind to the gate component. This allows the circuit to be reused without an additional toehold-based reset because the low energy bias allows the strands to be exchanged in either direction.

Furthermore, we developed a dual-rail TCR unit capable of continuously processing two distinct DNA inputs, representing the binary states 0 and 1 (Fig. 1C). Basic single-rail TCR units encode binary states in the presence or absence of a single-DNA-strand input, which requires fewer strands and a simpler design, thereby enabling faster propagation. However, single-rail units suffer from transient outputs between 0 and 1 when no input is present, which makes distinct binary outputs challenging. Therefore, the proposed dual-rail TCR unit incorporates dedicated gates and signal strands for each state. It consists of three gate components (gate 0, gate 1, and reporter) and two signal components corresponding to 0 and 1. The migration of these signal components is determined by the input. In contrast to conventional TMSD-based systems, inputs can be introduced to a circuit that has previously processed an input, which initiates a cascade of component migrations, thereby causing competition between the signal components for reporter binding. The displaced components of the past signal are inactivated by complementary

[1]Department of Materials Science and Engineering, Gwangju Institute of Science and Technology (GIST), Gwangju, Republic of Korea. [2]GIST InnoCORE AI-Nano Convergence Institute for Early Detection of Neurodegenerative Diseases, Gwangju Institute of Science and Technology, Gwangju, Republic of Korea. [3]School of Biological Sciences and Technology, Chonnam National University, Gwangju, Republic of Korea. [4]Department of Biological Chemistry and Molecular Pharmacology (BCMP), Harvard Medical School, Boston, MA, USA. [5]Graduate School of Engineering Biology, KAIST, Daejeon, Republic of Korea. [6]KI for Bioinnovation, KAIST, Daejeon, Republic of Korea.
*Corresponding author. Email: yeongjae@kaist.ac.kr
†These authors contributed equally to this work.

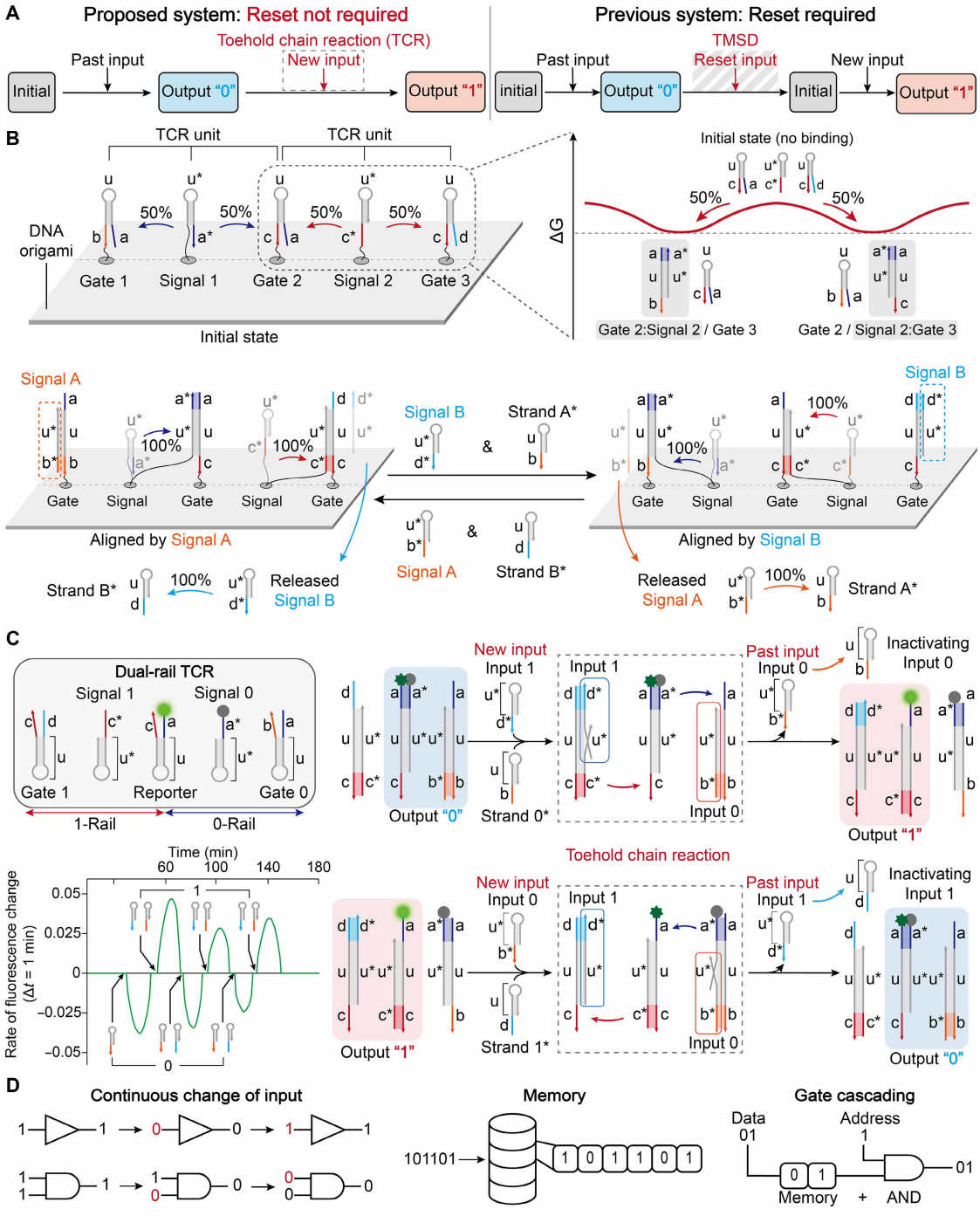

Fig. 1. TCR-based DNA logic circuits eliminate the need for reset steps, enabling continuous input processing and memory operation. (**A**) Comparison of the proposed and previously reported DNA logic circuit systems. The proposed system processes new inputs via TCR without a reset step, unlike previous systems that require a Reset input before each input processing step. (**B**) Cascaded TCR units on a DNA origami surface, which spatially localize components to prevent undesired reactions. Each TCR unit consists of a signal strand that can bind to two adjacent gates with an equal probability, as illustrated in the energy landscape diagram. These units enable directional and reversible alignment of signal strands in response to external input signals. The TCR units are directionally aligned by the introduction of a new input (Signal A or B) and a complementary strand (Strand A* or B*) that inactivates the past input. This reaction is reversible and proceeds without consuming the TCR components, allowing continuous, reset-free signal processing. (**C**) Composition of the dual-rail TCR system and output switching triggered by a new input. Two overlapping TCR units share a reporter strand. To switch the output, a new input is introduced along with a complementary strand that inactivates the past input signal. Input signals 0 and 1 and complementary strands were alternately applied to the TCR circuit while fluorescence was monitored, and the temporal derivative of fluorescence intensity was computed and plotted. To minimize background noise, all derivative values below a threshold of 0.01 were set to zero (see Materials and Methods for details). To overcome potential signal degradation from accumulated strands in solution, the concentration of each new input set was 1.1 times that of the past set. (**D**) Examples of logic circuits incorporating TCRs. TCR-based logic circuits support continuous input processing, memory capabilities, and cascading of logic gates.

strands, which are introduced alongside the new inputs (fig. S1). The direction of migration of the signal components was observed using fluorescence analysis (Fig. 1C and fig. S2), and the instantaneous reaction trends were quantitatively identified using differential analysis over time. Complex logic operations beyond simple strand migration can be achieved by leveraging the core mechanism of the dual-rail TCR unit, which uses bidirectional signal propagation driven by competitive strand displacement rather than separate reset steps.

Here, we proposed a TCR-based logic circuit as a versatile framework for reset-free processing by implementing logic gates and building cascaded connections (Fig. 1D). The TCR operating system permits simple designs, which makes it highly scalable and suitable for a wide range of logic circuits. We designed unique TCR structures and demonstrated a logic circuit capable of processing real-time inputs without a reset process that is scalable to complex circuits. We implemented basic combinational logic circuits (AND and OR gates), memory circuits (set-reset and data latches, termed SR- and D-latches, respectively), and a cascaded circuit combining an AND gate with a D-latch.

RESULTS

Reset-free and real-time operation of TCR-based logic gates

The TCR-based logic circuits were scaled up by using two-dimensional DNA origami templates to localize the DNA strands in the TCR unit, which minimized unintended interactions and enabled the operation of multiple circuits within a single origami structure (figs. S3 to S5 and Fig. 2A). In a solution-phase environment where all components are mixed, numerous gate and signal components can interact nonspecifically (*36*). By using DNA origami templates, molecular components can be spatially localized with nanometer-level precision, thereby minimizing undesired system leakage. This method also allows the reuse of identical component sequences at different positions on the template to enhance the overall scalability (*37*–*39*). DNA origami templates act as substrates that spatially control TCR reaction units, confining their interactions to specific locations, analogous to electronic circuit boards. This setup ensures that reactions only occur within the intended origami areas. Cross-talk experiments confirmed that the circuits operated exclusively within the individual origami structures (fig. S6). Furthermore, the TCR design incorporated a universal branch-domain sequence that folded into a hairpin at room temperature to suppress nonspecific interactions between components with noncomplementary toeholds and enabled competitive strand displacement of components (fig. S7). The TCR unit consisted of two gate components with a single signal component positioned between them, and an input complementary to the gate component determined the migration direction of the signal.

By modifying dual-rail TCR units on a DNA origami structure, we implemented basic logic gates, AND and OR gates. AND gates process two inputs {A, B} to produce one output (O); specifically, they produce an output of 1 only when both inputs are 1 (Fig. 2B). By engineering TCR unit variants with defined input thresholds, we produced logic gates that generated distinct responses to different input combinations. The TCR unit consisted of two gate components with a single signal component positioned between them, and an input complementary to the gate component determined the migration direction of the signal. The TCR circuits uniquely modified the input threshold required to determine the migration direction by adjusting the number of gate components accessible to the signal component. Therefore, we designed a TCR unit that exhibited two distinct threshold behaviors. The single-threshold TCR unit consisted of three gates and two signal components. Each signal component migrated exclusively between its two complementary gate components, and only one complementary input was required to determine the migration direction. Conversely, the double-threshold TCR unit consisted of three gate components and a single signal component that was complementary to all three gate components. Therefore, the migration direction in the double-threshold unit was determined only when two distinct inputs hybridized with the two gate components.

We implemented the AND gate using two different TCR units, and binary inputs were differentiated by leveraging their distinct threshold characteristics. All the TCR units shared a common gate component with the signal components competing for binding, which was termed the reporter. By combining single- and double-threshold TCR units, the migration directions of the signal components could be controlled depending on the specific input combinations, which enabled precise binary discrimination within the AND gate. The single-threshold TCR unit aligned the 0-signal component toward the reporter when either input A0 or B0 was present, whereas the double-threshold TCR unit aligned the 1-signal component toward the reporter when inputs A1 and B1 were both present (Fig. 2C and fig. S8). The OR gate was constructed with a single-threshold TCR unit, aligning the 1-signal toward the reporter if either input A1 or B1 was present, and a double-threshold TCR unit, which aligned the 0-signal component toward the reporter only when both inputs A0 and B0 were present; thus, 0 was output only when both inputs were 0 and 1 for all other combinations (Fig. 2D).

The AND and OR gates also processed changes to all four possible input combinations in real time, at 30-min intervals over 10 consecutive cycles, without requiring an additional reset process (Fig. 2, E and F). Furthermore, by differentiating the fluorescence with respect to time, we identified instantaneous reaction trends. By exploiting a mechanism in which the signal components of two unit types are competitively displaced, dictating their migration path and output, we implemented fundamental logic gates and validated the circuit reusability and responsiveness. Moreover, by adjusting the number of gates and signal components in the TCR units, this system can be extended to implement multiple-input logic gates.

SR-latch implementation using a single-strand concatenated TCR architecture

With reset-free data processability, TCR overcomes the limitations of traditional DNA computing, which is confined to combinational logic circuits, and extends its application to memory circuits capable of processing information in real time. Unlike combinational logic circuits that determine outputs based solely on the current inputs, memory circuits produce outputs by considering sequential inputs. However, memory circuits have not been implemented in DNA computing because strand displacement–based DNA computing requires a reset step to return the circuit to its initial state before processing new inputs. Although previous studies have attempted to develop temporal logic circuits and memory circuits on the basis of DNA logic gates, these approaches either lack reusability (*40*, *41*) or require manual intervention beyond DNA inputs during data processing (*30*, *42*). Therefore, we used TCRs to implement SR- and D-latches, fundamental memory circuits capable of storing information.

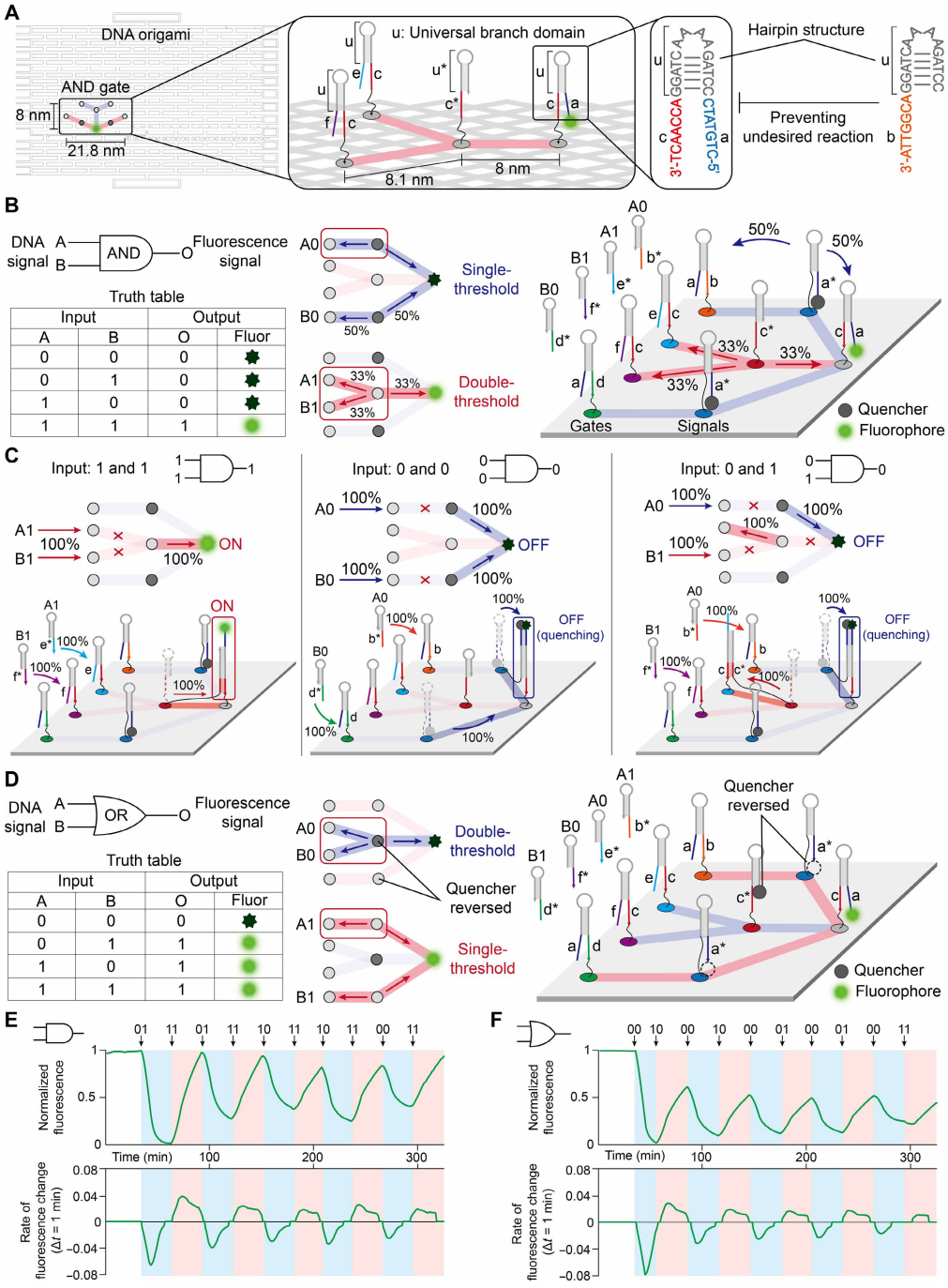

Fig. 2. TCR-based AND and OR gates. (**A**) The components of the TCR units were positioned at uniform intervals on the DNA origami structure. Each DNA probe consisted of two processing domains and a universal branch domain, denoted as "u," which had an identical sequence and adopted a hairpin structure when not hybridized. (**B**) Truth table and schematic of the TCR-based AND gate using a modified dual-rail system. Single-threshold units containing a quencher were activated by a single input and produced an OFF output. Double-threshold units lacked a quencher and required two identical inputs to generate an ON output. Percentages represent the theoretical competitive binding probabilities between signal and adjacent gate strands. (**C**) Schematics of the TCR-based AND gate operation for each input combination. Inputs bind selectively to designated gates, causing the signal strands to align along the unoccupied strands. (**D**) Truth table and schematic of the TCR-based OR gate using a modified dual-rail system. The OR gate can be implemented by reversing the positions of the quenchers used in the AND gate. (**E** and **F**) Output of the AND gate (E) and OR gate (F) in response to continuous input combinations. Fluorescence intensities were measured and normalized over time to evaluate circuit behavior. Input combinations {A, B} were applied to the TCR circuit while fluorescence was monitored, and the temporal derivative of fluorescence intensity was computed and plotted. To ensure a robust state transition, the input concentration was increased by 1.1 times in each cycle. The colored background represents the output state for each input combination: Blue indicates an output of "0" (OFF state), and red indicates an output of "1" (ON state). To minimize background noise, all derivative values below a threshold of 0.01 were set to zero (see Materials and Methods for details).

We implemented an SR-latch by designing the gate components of the "Reset" and "Set" dual-rail TCRs to be concatenated onto a single, integrated DNA strand. This design allowed the Reset dual-rail TCR to regulate the operation of the Set dual-rail TCR (Fig. 3A). This concatenation is the key to achieving the memory function. By concatenating two TCR units onto a single strand, the activation of one unit by an input triggers a strand displacement reaction that selectively opens one toehold while closing the other. This shift in toehold accessibility directly determines whether a second TCR unit accepts its input. Therefore, the circuit's response to a new input becomes dependent on the state Set by a past input, enabling the "Hold" operation fundamental to a memory circuit. An SR-latch calculates

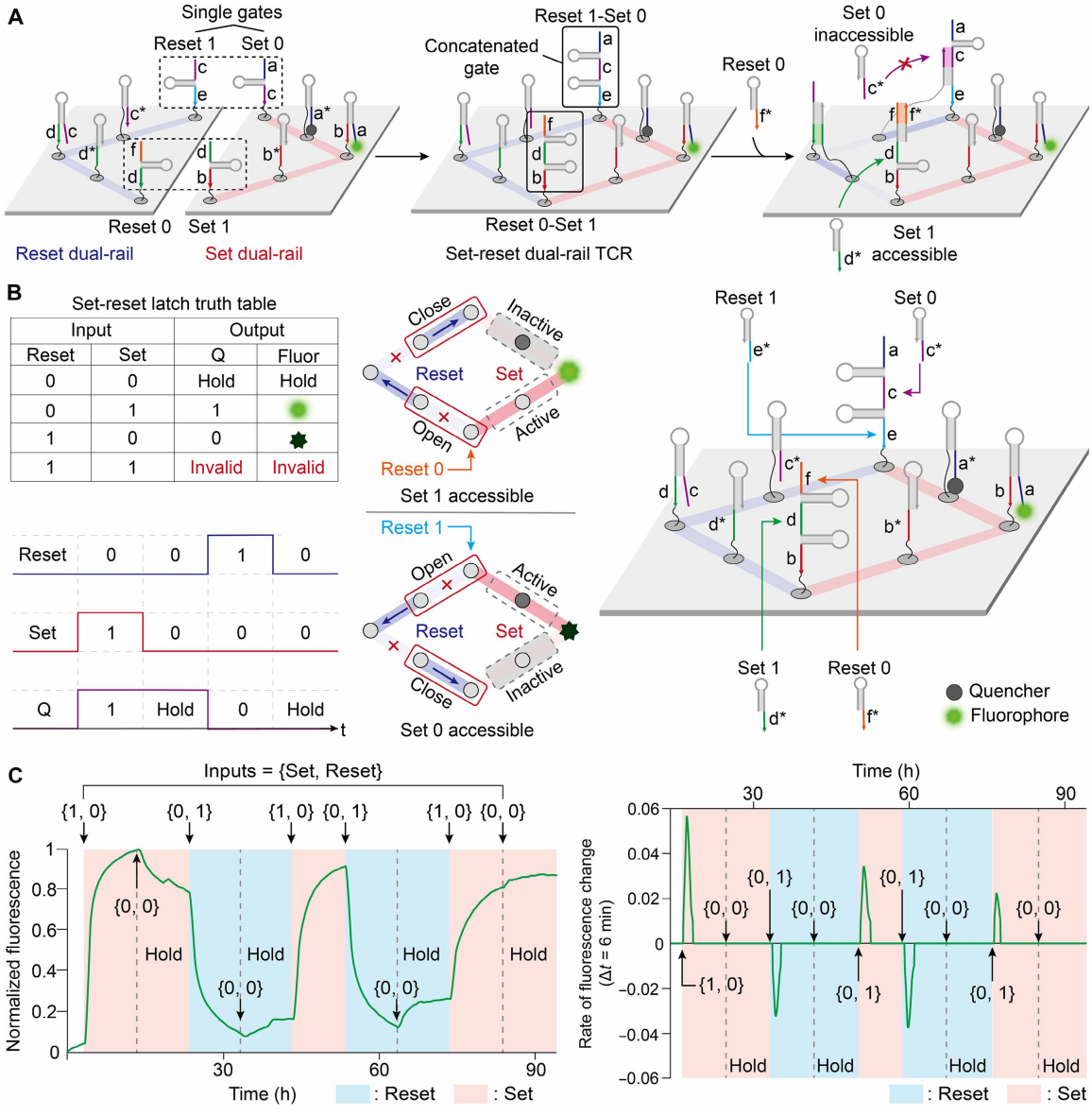

Fig. 3. TCR-based SR-latch. (**A**) Formation and operation of the concatenated dual-rail TCR-based structure. The reset and set dual-rail TCRs were concatenated to allow a coordinated response to both inputs. Following the "Reset" input, signal alignment via a toehold-mediated reaction regulated the Set signal accessibility, which controlled the activation of the opposing TCR unit. (**B**) Truth table of the TCR-based SR-latch and illustration of the concatenated dual-rail TCR system on a DNA origami structure. The SR-latch operated on the basis of two inputs, "Set" and "Reset." The Reset signal was introduced to one side of the gate, which initiated signal component alignment within the reset dual-rail TCR. Consequently, the gate that received the Reset signal became accessible to the Set signal, whereas the opposite gate became inaccessible. When the Set signal was introduced to the accessible gate, it determined whether the output was switched ON or OFF. (**C**) Output of the SR-latch in response to continuous input combinations. The fluorescence intensities were measured and normalized over time to evaluate circuit behavior. Input combinations {Set, Reset} were applied to the TCR circuit while fluorescence was monitored, and the temporal derivative of fluorescence intensity was computed and plotted. To ensure robust state transitions and drive the reaction to completion, the input concentration was increased by 1.1 times in each cycle. The colored background represents the output state for each input combination: Blue indicates an output of "Reset," and red indicates an output of "Set." To minimize background noise, all derivative values below a threshold of 0.01 were set to zero (see Materials and Methods for details). h, hour.

its output using two inputs: "Set" and "Reset" (Fig. 3B). The Set input drives the output to 1, whereas the Reset input drives the output to 0. When the Set and Reset inputs are both 0, the latch retains its previous state. This function is termed the hold operation. The hold operation enables the circuit to maintain outputs that are dependent on prior states, thereby preserving the memory despite receiving new inputs. The gate components of both TCRs shared a single overlapping toehold domain. The signal component of the reset dual-rail TCR, which shared this toehold with the input of the set dual-rail TCR, occupied the domain and prevented the Set input from binding. Consequently, when the reset dual-rail TCR received an input and its signal components aligned in one direction, one of the two gate components was occupied by the signal component of the reset dual-rail TCR, which blocked the Set input, whereas the other gate component remained accessible to the Set input. In the TCR-based SR-latch, the set dual-rail TCR outputs a signal component identical to the Set input, whereas the reset dual-rail TCR blocks the toehold domain for the Set input that matched the Reset input and simultaneously opens the toehold domain for the Set input opposite to the Reset input. Specifically, Reset input 0 opened the toehold domain for Set input 1, and Reset input 1 opened the toehold domain for the Set input 0 signal (fig. S9). Therefore, when the Reset and Set inputs differed (R, S = 0, 1 or 1, 0), the SR-latch outputs the value of the Set input. If the Set and Reset inputs were both 0, the reset dual-rail TCR blocked the toehold domain required by the Set input 0, which prevented the activation of the set dual-rail TCR; therefore, the SR-latch remained in its previous state. This concatenated configuration enables implementation of an SR-latch capable of real-time, one-bit information control across all three valid input combinations.

SR-latch reliably performed essential memory operations in the sequence (Set → Hold → Reset → Hold → Set → Reset → Hold → Set → Hold), updating and maintaining the output across nine sequential cycles without requiring resets (Fig. 3C). This demonstrates robust real-time processing of inputs under all valid input scenarios. Fluorescence changes observed within the first 20 min following input introduction represented ~40% of the total 10-hour signal, and fluorescence-based differential analysis, using a 60-min sliding difference, enabled precise characterization of instantaneous reaction dynamics and trends.

D-latch implementation using a single-strand concatenated TCR architecture

Next, we implemented a D-latch (Fig. 4A) designed to address the unintuitive operation and inability to process certain input combinations. The D-latch produced outputs on the basis of the Data and Enable inputs. The Enable input determined whether the D-latch retained its previous state or was updated to a new value, whereas the Data input defined the output value of the D-latch. This functionality was accomplished by integrating two "Enable" TCR units with the gate components of the Data dual-rail TCR. Specifically, each of the two nonreporter gates in the Data dual-rail TCR was designed as a single concatenated DNA strand that also included an Enable TCR unit.

By concatenating an Enable TCR unit and a Data gate onto a single strand, activation of the Enable TCR unit by an input triggers a strand displacement reaction that selectively opens or closes a shared toehold. This shift in toehold accessibility directly determines whether the Data gate can accept the Data input. The two signal components of the Enable TCR units and the inputs of the Data dual-rail TCR unit shared a common toehold (fig. S10). Consequently, when either the Enable signal component or Data input occupied this shared toehold, the other was prevented from binding or reacting. Therefore, by regulating the alignment of the Enable TCR signal components via the Enable input, the Enable TCR units controlled whether the Data input activated the Data TCR unit, thereby determining the latch output. Hence, this integrated architecture, where each Data gate is physically linked to its own Enable unit, created a memory circuit that could switch seamlessly between the read and write modes.

The D-latch alternated between active and inactive modes over nine cycles without resetting (Fig. 4B). In the active mode, an input of 0 to 1 updated the output; in the inactive mode, the same inputs were ignored, and when active again, an input of 0 to 1 updated the output. The implemented D-latch processed real-time inputs across nine sequential cycles without requiring a reset. Fluorescence intensity changes observed within 20 min after input introduction accounted for ~40% of the total fluorescence variation measured throughout the entire 7-hour cycle, and fluorescence-based differential analysis, using a 40-min sliding difference, enabled precise characterization of instantaneous reaction dynamics and trends.

TCR-based register integrating logic and memory functions

Last, to demonstrate the scalability of the TCR, we implemented a register that combined a combinational logic circuit with a memory circuit that could process multiple sequential inputs (Fig. 5A). The register consisted of two 1-bit memory cells. Each 1-bit memory cell was constructed by integrating a D-latch with an AND gate. Specifically, two Enable TCR units were concatenated onto one gate component of a single-threshold TCR unit and one gate component of a double-threshold TCR unit in the AND gate. The register operated using an input address signal, 1-bit input data, and an output address signal. The input address activated the corresponding 1-bit memory cell for writing, the 1-bit data were stored in that cell, and the output address retrieved the data held in the selected memory cell (Fig. 5B and fig. S11).

The implemented register with two 1-bit memory cells produced correct outputs for all the input combinations and sequentially processed real-time inputs over five cycles without requiring a reset (Fig. 5C). Within 20 min following input introduction, ~40% of the total fluorescence change was observed.

DISCUSSION

In this study, we introduced a DNA logic circuit framework using TCRs as a foundational mechanism. The proposed TCR-based system uniquely exploited the reversible and competitive strand displacement of DNA strands with comparable binding affinities, which enabled continuous information processing and memory operations. Specifically, the reversible nature of TCRs facilitated the dynamic realignment of signal strands in response to inputs without inducing structural changes that could not be reversed without external stimuli. This contrasts with traditional TMSD circuits, which require additional secondary domains to reset the states that increase the complexity and hinder scalability, particularly in cascaded circuit configurations.

The reusability and real-time input processing capabilities of the TCR framework were demonstrated using dual-rail TCR units that discriminated binary states via dedicated gates and signal components. Beyond fundamental logic gates, we realized advanced memory circuits

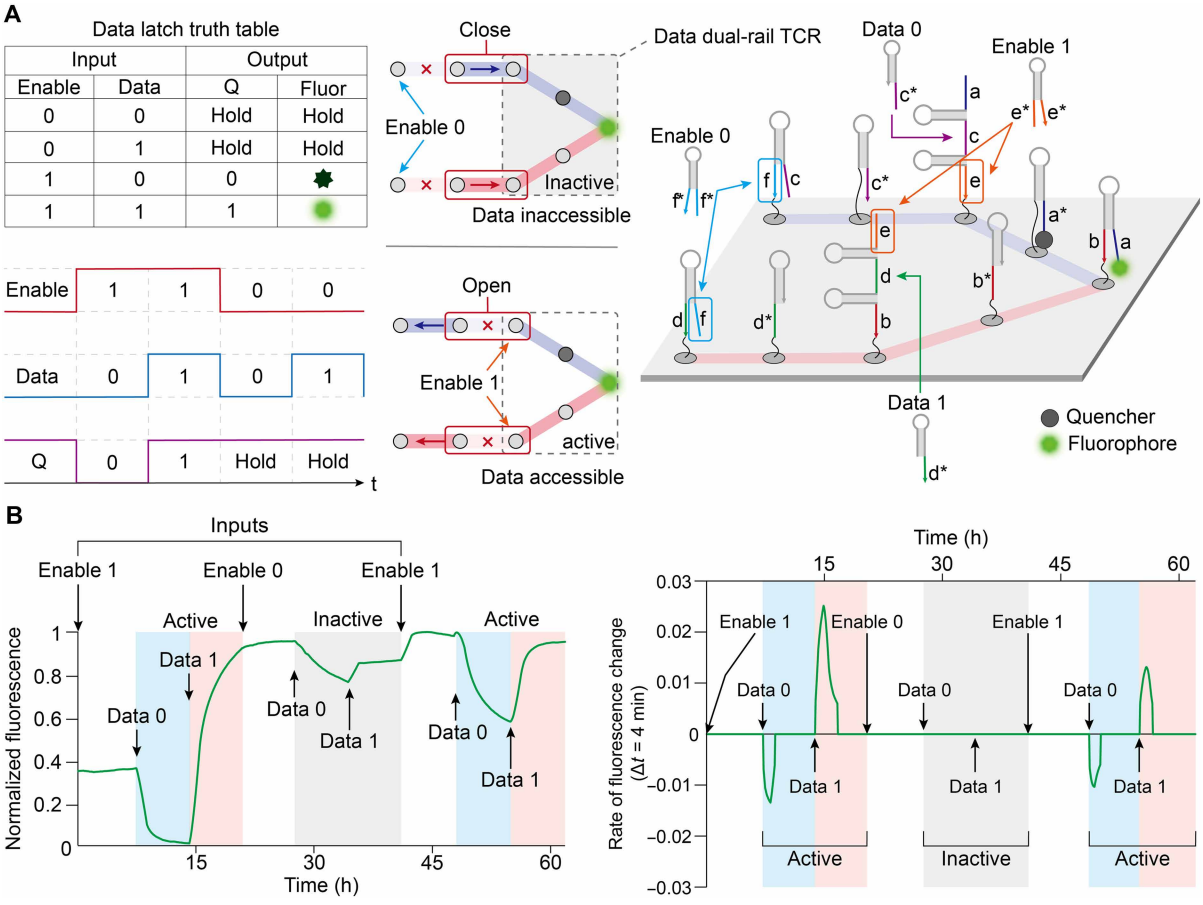

Fig. 4. TCR-based D-latch. (**A**) Truth table of the TCR-based D-latch and illustration of the dual-rail TCR system on a DNA origami structure. The D-latch contained an additional TCR unit placed downstream of each rail in the dual-rail TCR. These auxiliary units controlled whether the dual-rail TCR remained active or inactive. "Enable" and "Data" inputs were introduced via an additional toehold domain in the central gate component. (**B**) Output of the D-latch in response to continuous input combinations. The fluorescence intensities were measured and normalized over time to evaluate the circuit behavior. Inputs (Enable, Data) were applied to the TCR circuit while fluorescence was monitored, and the temporal derivative of fluorescence intensity was computed and plotted. To ensure robust state transitions and drive the reaction to completion, the input concentration was increased by 1.1 times in each cycle. The colored background represents the operational state of the D-latch: Blue and red indicate transition to output "0" and "1" in the "Active" state, respectively, and gray indicates the "Inactive" state. To minimize background noise, all derivative values below a threshold of 0.01 were set to zero (see Materials and Methods for details).

such as the SR- and D-latches using concatenated TCR units and implemented a register by combining these memory elements with combinational logic. However, the TCR-based framework has limitations. First, its reaction kinetics are inherently slower than those of irreversible TMSD-based circuits. This slowness is primarily because all gate and signal components use hairpin structures to reduce nonspecific interactions. The need to unfold these secondary structures makes the DNA hybridization process less efficient (*43*). Second, the system exhibits minor signal leakage because of incomplete strand displacement. In our experiments, new input strands and strands complementary to the past input were introduced at concentrations incrementally increased by 10% in each cycle to compensate for the incomplete inactivation of prior inputs and to maintain reliable state transitions in the TCR circuit. While this strategy preserves robust processing behavior, it simultaneously accelerates the accumulation of inert waste complexes formed from previous input-complementary strand interactions. This accumulation represents the factor limiting the total number of achievable reuse cycles, as it creates a congested molecular environment that hinders the diffusion and interaction of active components. As a result, the system exhibits a gradual decrease in both signal amplitude and reaction efficiency over multiple cycles.

Optimizing the circuit design by enhancing the sequence specificity of toeholds and diversifying the sequences of the universal branch domains to eliminate the need for secondary hairpin structures results in faster reactions, improved reusability, deeper circuit architectures, and shorter intervals required for reliable signal propagation. If simulation tools can capture the dynamic and transient behavior of TCR reactions, researchers can implement more accurate, scalable rational circuit designs by incorporating precise experimental variables.

The scalability of the memory circuit using our system is suitable for advanced computational functions such as dynamic data storage, sequential decision-making, and adaptive responsiveness. This substantially broadens the potential applications of DNA-based computing and extends them to DNA-driven artificial intelligence. Furthermore, our TCR-based framework provides a solid foundation for practical applications in biomedical diagnostics, targeted therapeutics, and synthetic biology.

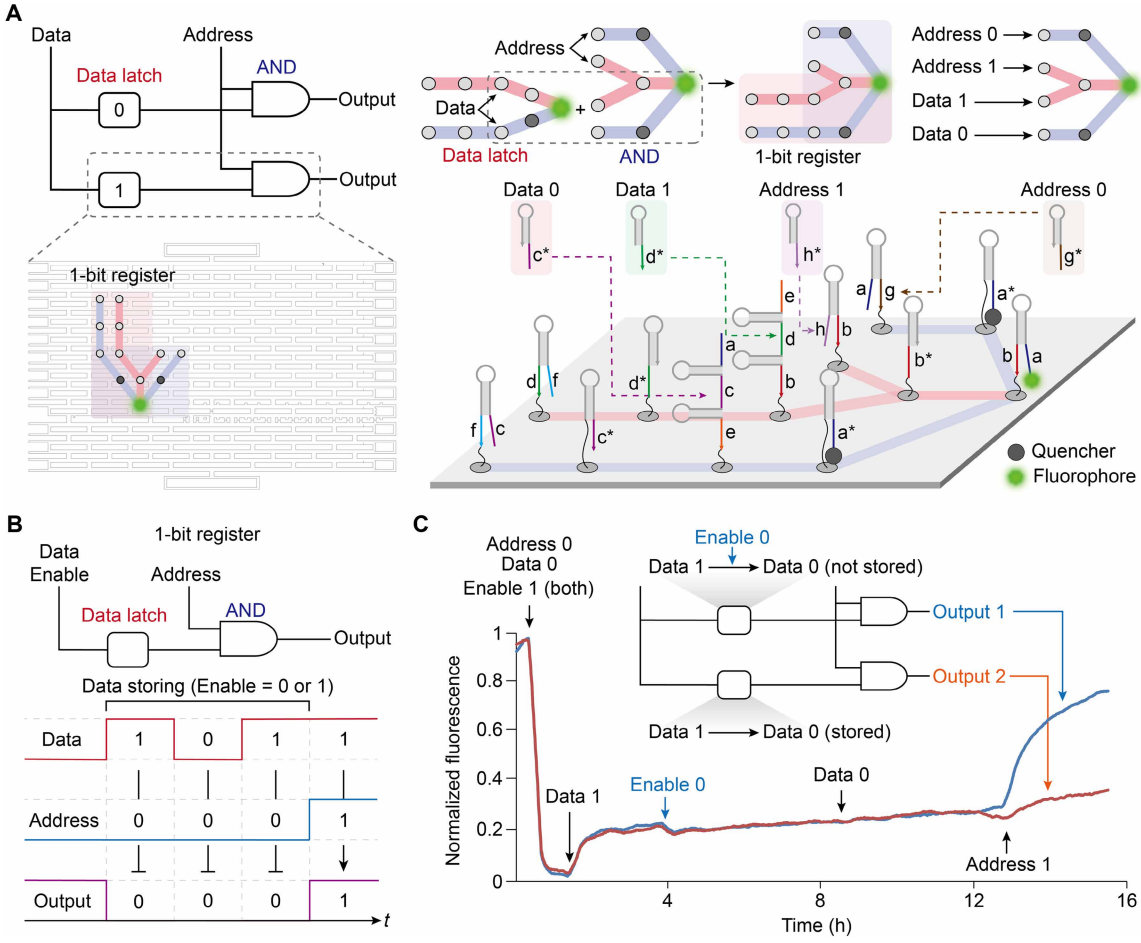

Fig. 5. TCR-based register. (**A**) Circuit of the TCR-based register and illustration of the TCR system on a DNA origami structure. The TCR-based register was implemented by combining one D-latch and one AND gate. The D-latch functioned to store the Data input, whereas the AND gate determined whether the stored value in the D-latch was output. Among the four rails of the AND gate, half received the Address input, and the other half received the Data input. TCR-based registers were localized on a single DNA origami structure, which allowed the storage of 1-bit data. (**B**) Operation of the 1-bit TCR-based register. The Data input was introduced to store data in the register. When the Address input was 0, the final output did not reflect any changes. When the Address input switched to 1, the output corresponded to the value stored in the D-latch. (**C**) Output of two parallel connected 1-bit registers in response to continuous inputs. Fluorescence signals were measured at defined time intervals as different combinations of Data, Enable, and Address inputs were introduced sequentially. The fluorescence intensities were normalized and plotted over time to monitor the behavior of the circuit.

MATERIALS AND METHODS

Materials

The M13mp18 single-stranded DNA scaffold was purchased from New England Biolabs (cat. no. N4040S). The circuit probes, inputs, and staple oligonucleotides with extensions were purchased from Macrogen (Seoul, South Korea). DNA oligonucleotides without fluorophores or quenchers were purified using a Macrogen oligonucleotide purification cartridge, and labeled DNA oligonucleotides with fluorophores [FAM (6-carboxyfluorescein) and HEX (hexachlorofluorescein)] or quenchers [BHQ1 (Black Hole Quencher 1)] were purified using polyacrylamide gel electrophoresis by Macrogen. Detailed sequences are shown in tables S1 to S10. Streptavidin was purchased from Thermo Fisher Scientific, South Korea (cat. no. 434301).

Sequence design process

All DNA sequences used in the TCR-based circuits consist of a 14-nucleotide universal branch domain and a 7-nucleotide unique toehold domain. The signal component is composed of one universal branch domain and one unique toehold domain. Gate components of the combinational logic circuits contain one universal branch domain and two unique toehold domains, whereas those of memory circuits consist of two universal branch domains and three unique toehold domains. To suppress undesired strand interactions arising from the universal branch domain, this region is designed to spontaneously form a secondary hairpin structure at 37°C.

The design of unique toehold domains is critical for the reversibility of the TCR, which relies on a low and balanced energy barrier for strand displacement in forward and reverse directions. To achieve this, an iterative algorithm governed by three key rules was used. First, to ensure comparable binding affinities and prevent a strong thermodynamic bias that would inhibit reversibility, all toehold sequences were designed to be seven nucleotides long and to have a consistent GC content (exactly three G or C bases). Second, each designed DNA strand was validated using NUPACK to ensure the

absence of undesired secondary structures (*44*, *45*). Last, to minimize nonspecific interactions and cross-talk, each new sequence was required to have at least a 50% nucleotide difference (a Hamming distance ≥4) from all previously accepted sequences in the library. The design process followed an iterative loop of generation and validation until a sequence satisfying all criteria was generated (fig. S12).

DNA origami assembly process

A DNA scaffold (10 nM) was mixed with 8 times excess of the regular staple strands and 20 times excess of the modified staple strands in 1× tris-acetate-EDTA (TAE)/Mg^{2+} buffer [40 mM tris, 20 mM acetic acid, 2 mM EDTA, and 12.5 mM $MgCl_2$]. The annealing was processed with a polymerase chain reaction thermocycler (C1000 Touch Thermal Cycler). The procedure was set as follows: The sample was first heated up to 95°C and incubated for 15 min, then slowly cooled to 20°C at 1°C every 1 min, incubated at 20°C for 5 min, and then held at 4°C. After annealing, folded origami samples were then purified using 0.5-ml, 100-kDa spin filters (Amicon, Germany) each time for 20 min at 2000*g*.

AFM measurements

Samples for atomic force microscopy (AFM) imaging were first purified with 100-kDa Amicon spin filters and then incubated with 20-fold excess of streptavidin protein for 1 hour at room temperature. For AFM imaging, 10 μl of the samples was deposited onto a freshly cleaved mica surface (Ted Pella, US) for 10 min. The mica surface was then washed twice with nuclease-free water using compressed air. After washing, the samples were imaged in noncontact mode of an FX-40 AFM (Park Systems, Republic of Korea) using NCHR-50 probes (NANO WORLD, Switzerland). The 2 μm–by–2 μm and 500 nm–by–500 nm AFM images were scanned at a resolution of 256 pixels by 256 pixels and a scan rate of 0.5 Hz.

Gel electrophoresis for purification characterization

To analyze the purification efficiency, 1.5% agarose gel was prepared by mixing 0.9 g of agarose (BioFact Co., South Korea) in 60 ml of 1× TAE/Mg^{2+} buffer. The solution was then heated in a microwave oven for 3 min and cooled to ~50°C before pouring it into the gel tray. After solidifying, the gel was placed in the gel tray in a container with ice. TAE/Mg^{2+} buffer (1×) was used as running buffer. The samples with 1× SYBR Safe were loaded into agarose gels and subjected to gel electrophoresis at 70 V for 2 hours.

Fluorescence kinetics experiments

Kinetic fluorescence was measured using a CFX Connect Real-Time PCR Detection System and a CFX Opus 96 Real-Time PCR System (Bio-Rad Laboratories), with all measurements performed consistently at 37°C. The fluorescence of the samples was measured at 510 nm (excitation) and 540 nm (emission). For the initial reaction, input strands were introduced to reach a final concentration of 200 nM—a 10-fold excess relative to the DNA origami. In subsequent cycles, the new input and its complementary strand were added at 1.1 times the previous input amount to maintain robustness. During experiments, each cycle was temporarily paused to manually introduce input DNA strands and gently mix the contents before the measurement was resumed. Fluorescence kinetics for each experiment were detected at intervals of 1 min (Figs. 1C; 2, E and F; and 5C and fig. S6), 4 min (Fig. 4B and fig. S4), 5 min (fig. S2), and 6 min (Fig. 3C).

Postprocessing of fluorescence traces

We normalized the fluorescence signals to relative output levels, defining the minimum level (output = 0) as the lowest value observed across all measurements and the maximum level (output = 1) as the highest value observed in the experiment. Normalized fluorescence time series were first smoothed using a Savitzky-Golay filter (window length of 10 cycles and polynomial order of 1) to suppress high-frequency noise introduced during manual tube handling (*46*). The smoothed signal $F_s(t)$ was then differentiated with the same filter settings (first derivative, $\Delta t = 1$ cycle) to yield the kinetic rate of fluorescence change, dF_s/dt. Last, minor fluctuations were removed by setting all $|dF_s/dt|$ values below 0.01 (relative fluorescence units per cycle) to zero. This workflow ensures that only genuine kinetic transitions remain for further analysis.

Supplementary Materials

The PDF file includes:

Figs. S1 to S12
Tables S1 to S9
Legend for data S1

Other Supplementary Material for this manuscript includes the following:

Data S1

REFERENCES

1. Y. Zhang, X. Yin, C. Cui, K. He, F. Wang, J. Chao, T. Li, X. Zuo, A. Li, L. Wang, N. Wang, X. Bo, C. Fan, Prime factorization via localized tile assembly in a DNA origami framework. *Sci. Adv.* **9**, eadf8263 (2023).
2. H. Lv, N. Xie, M. Li, M. Dong, C. Sun, Q. Zhang, L. Zhao, J. Li, X. Zuo, H. Chen, F. Wang, C. Fan, DNA-based programmable gate arrays for general-purpose DNA computing. *Nature* **622**, 292–300 (2023).
3. K. N. Lin, K. Volkel, C. Cao, P. W. Hook, R. E. Polak, A. S. Clark, A. S. Miguel, W. Timp, J. M. Tuck, O. D. Velev, A. J. Keung, A primordial DNA store and compute engine. *Nat. Nanotechnol.* **19**, 1654–1664 (2024).
4. J. J. Shu, Z. H. Tan, Q. W. Wang, K. Y. Yong, Programmable biomolecule-mediated processors. *J. Am. Chem. Soc.* **145**, 25033–25042 (2023).
5. W. Kim, M. Chon, Y. Koh, H. Choi, E. Choi, H. Park, Y. Jung, T. Ryu, S. Kwon, Y. Choi, Oligonucleotide subsets selection by single nucleotide resolution barcode identification. *Nat. Commun.* **16**, 1586 (2025).
6. Q. Ma, M. Zhang, C. Zhang, X. Teng, L. Yang, Y. Tian, J. Wang, D. Han, W. Tan, An automated DNA computing platform for rapid etiological diagnostics. *Sci. Adv.* **8**, eade0453 (2022).
7. X. K. Lun, K. Sheng, X. Yu, C. Y. Lam, G. Gowri, M. Serrata, Y. Zhai, H. Su, J. Luan, Y. Kim, D. E. Ingber, H. W. Jackson, M. B. Yaffe, P. Yin, Signal amplification by cyclic extension enables high-sensitivity single-cell mass cytometry. *Nat. Biotechnol.* **43**, 811–821 (2025).
8. J. Sun, X. Xiong, W. Lai, Z. Wu, H. Wang, L. Yang, N. Xue, Q. Yao, G. Song, Y. Zhao, L. Li, F. Wang, C. Fan, H. Pei, Implementing complex nucleic acid circuits in living cells. *Sci. Adv.* **11**, eadv6512 (2025).
9. G. Chen, D. Liu, C. He, T. R. Gannett, W. Lin, Y. Weizmann, Enzymatic synthesis of periodic DNA nanoribbons for intracellular pH sensing and gene silencing. *J. Am. Chem. Soc.* **137**, 3844–3851 (2015).
10. I. Kawamata, K. Nishiyama, D. Matsumoto, S. Ichiseki, J. J. Keya, K. Okuyama, M. Ichikawa, A. M. R. Kabir, Y. Sato, D. Inoue, S. Murata, K. Sada, A. Kakugo, S. M. Nomura, Autonomous assembly and disassembly of gliding molecular robots regulated by a DNA-based molecular controller. *Sci. Adv.* **10**, eadn4490 (2024).
11. M. Kim, C. Lee, K. Jeon, J. Y. Lee, Y. J. Kim, J. G. Lee, H. Kim, M. Cho, D. N. Kim, Harnessing a paper-folding mechanism for reconfigurable DNA origami. *Nature* **619**, 78–86 (2023).
12. Y. Kim, P. Yin, Enhancing biocompatible stability of DNA nanostructures using dendritic oligonucleotides and brick motifs. *Angew. Chem. Int. Ed. Engl.* **59**, 700–703 (2020).
13. A. E. Gerdon, S. S. Oh, K. Hsieh, Y. Ke, H. Yan, H. T. Soh, Controlled delivery of DNA origami on patterned surfaces. *Small* **5**, 1942–1946 (2009).
14. F. Hong, S. Jiang, T. Wang, Y. Liu, H. Yan, 3D framework DNA origami with layered crossovers. *Angew. Chem. Int. Ed. Engl.* **55**, 12832–12835 (2016).
15. Y. Choi, H. Choi, A. C. Lee, H. Lee, S. Kwon, A reconfigurable DNA accordion rack. *Angew. Chem. Int. Ed. Engl.* **57**, 2811–2815 (2018).

16. J. Roh, S. Park, H. Kim, W. Kim, J. Kim, C. Park, H. Choi, S. Song, E. Choi, Y. Choi, Polymorphing hydrogels regulated by photo-reactive DNA cross-links. *Adv. Mater.* **37**, e2414648 (2025).
17. K. M. Cherry, L. Qian, Scaling up molecular pattern recognition with DNA-based winner-take-all neural networks. *Nature* **559**, 370–376 (2018).
18. X. Xiong, T. Zhu, Y. Zhu, M. Cao, J. Xiao, L. Li, F. Wang, C. Fan, H. Pei, Molecular convolutional neural networks with DNA regulatory circuits. *Nat. Mach. Intell.* **4**, 625–635 (2022).
19. Y. Zhu, X. Xiong, M. Cao, L. Li, C. Fan, H. Pei, Accelerating DNA computing via freeze-thaw cycling. *Sci. Adv.* **9**, eaax7983 (2023).
20. A. J. Thubagere, W. Li, R. F. Johnson, Z. Chen, S. Doroudi, Y. L. Lee, G. Izatt, S. Wittman, N. Srinivas, D. Woods, E. Winfree, L. Qian, A cargo-sorting DNA robot. *Science* **357**, eaan6558 (2017).
21. J. Chao, J. Wang, F. Wang, X. Ouyang, E. Kopperger, H. Liu, Q. Li, J. Shi, L. Wang, J. Hu, L. Wang, W. Huang, F. C. Simmel, C. Fan, Solving mazes with single-molecule DNA navigators. *Nat. Mater.* **18**, 273–279 (2019).
22. J. Li, A. Johnson-Buck, Y. R. Yang, W. M. Shih, H. Yan, N. G. Walter, Exploring the speed limit of toehold exchange with a cartwheeling DNA acrobat. *Nat. Nanotechnol.* **13**, 723–729 (2018).
23. L. Qian, E. Winfree, Scaling up digital circuit computation with DNA strand displacement cascades. *Science* **332**, 1196–1201 (2011).
24. T. Song, A. Eshra, S. Shah, H. Bui, D. Fu, M. Yang, R. Mokhtar, J. Reif, Fast and compact DNA logic circuits based on single-stranded gates using strand-displacing polymerase. *Nat. Nanotechnol.* **14**, 1075–1081 (2019).
25. F. Wang, H. Lv, Q. Li, J. Li, X. Zhang, J. Shi, L. Wang, C. Fan, Implementing digital computing with DNA-based switching circuits. *Nat. Commun.* **11**, 121 (2020).
26. S. D. Lemaire, D. Turek, D. Landsman, M. Colotte, T. F. A. de Greef, Challenges and opportunities in DNA computing and data storage. *Nat. Nanotechnol.* **20**, 710–714 (2025).
27. X. Song, A. Eshra, C. Dwyer, J. Reif, Renewable DNA seesaw logic circuits enabled by photoregulation of toehold-mediated strand displacement. *RSC Adv.* **7**, 28130–28144 (2017).
28. J. Hahn, W. M. Shih, Thermal cycling of DNA devices via associative strand displacement. *Nucleic Acids Res.* **47**, 10968–10975 (2019).
29. X. Sun, D. Yao, H. Liang, pH-controlled resettable modular DNA strand-displacement circuits. *Nano Lett.* **23**, 11540–11547 (2023).
30. T. Xie, C. Li, M. Hu, X. Zhong, J. Xiao, Z. Zhang, Z. Wang, T. Wu, DNA sequential logic circuits for reversible counters and dynamic biomolecular sensing. *Adv. Sci.* **12**, e05793 (2025).
31. N. Srinivas, J. Parkin, G. Seelig, E. Winfree, D. Soloveichik, Enzyme-free nucleic acid dynamical systems. *Science* **358**, eaal2052 (2017).
32. F. C. Simmel, B. Yurke, H. R. Singh, Principles and applications of nucleic acid strand displacement reactions. *Chem. Rev.* **119**, 6326–6369 (2019).
33. S. Garg, S. Shah, H. Bui, T. Song, R. Mokhtar, J. Reif, Renewable time-responsive DNA circuits. *Small* **14**, e1801470 (2018).
34. Y. Liu, Y. Zhai, H. Hu, Y. Liao, H. Liu, X. Liu, J. He, L. Wang, H. Wang, L. Li, X. Zhou, X. Xiao, Erasable and field programmable DNA circuits based on configurable logic blocks. *Adv. Sci.* **11**, e2400011 (2024).
35. A. Eshra, S. Shah, T. Song, J. Reif, Renewable DNA hairpin-based logic circuits. *IEEE Trans. Nanotechnol.* **18**, 252–259 (2019).
36. H. Bui, S. Shah, R. Mokhtar, T. Song, S. Garg, J. Reif, Localized DNA hybridization chain reactions on DNA origami. *ACS Nano* **12**, 1146–1155 (2018).
37. G. Chatterjee, N. Dalchau, R. A. Muscat, A. Phillips, G. Seelig, A spatially localized architecture for fast and modular DNA computing. *Nat. Nanotechnol.* **12**, 920–927 (2017).
38. L. Liu, F. Hong, H. Liu, X. Zhou, S. Jiang, P. Šulc, J. H. Jiang, H. Yan, A localized DNA finite-state machine with temporal resolution. *Sci. Adv.* **8**, eabm9530 (2022).
39. Z. Tang, S. Li, C. Chen, Z. Zhou, Z. Yin, A localized scalable DNA logic circuit system based on the DNA origami surface. *Int. J. Mol. Sci.* **26**, 2043 (2025).
40. A. P. Lapteva, N. Sarraf, L. Qian, DNA strand-displacement temporal logic circuits. *J. Am. Chem. Soc.* **144**, 12443–12449 (2022).
41. M. Zhang, C. Yancey, C. Zhang, J. Wang, Q. Ma, L. Yang, R. Schulman, D. Han, W. Tan, A DNA circuit that records molecular events. *Sci. Adv.* **10**, eadn3329 (2024).
42. Q. Zhang, M. Li, Y. Tang, J. Zhang, C. Sun, Y. Hao, J. Cheng, X. Xie, S. Jia, H. Lv, F. Wang, C. Fan, High-speed sequential DNA computing using a solid-state DNA origami register. *ACS Cent. Sci.* **10**, 2285–2293 (2024).
43. Y. Gao, L. K. Wolf, R. M. Georgiadis, Secondary structure effects on DNA hybridization kinetics: A solution versus surface comparison. *Nucleic Acids Res.* **34**, 3370–3377 (2006).
44. J. N. Zadeh, C. D. Steenberg, J. S. Bois, B. R. Wolfe, M. B. Pierce, A. R. Khan, R. M. Dirks, N. A. Pierce, NUPACK: Analysis and design of nucleic acid systems. *J. Comput. Chem.* **32**, 170–173 (2011).
45. M. E. Fornace, J. Huang, C. T. Newman, N. J. Porubsky, M. B. Pierce, N. A. Pierce, NUPACK: Analysis and design of nucleic acid structures, devices, and systems. ChemRxiv (2022); https://doi.org/10.26434/chemrxiv-2022-xv98l-v2.
46. P. Virtanen, R. Gommers, T. E. Oliphant, M. Haberland, T. Reddy, D. Cournapeau, E. Burovski, P. Peterson, W. Weckesser, J. Bright, S. J. van der Walt, M. Brett, J. Wilson, K. J. Millman, N. Mayorov, A. R. J. Nelson, E. Jones, R. Kern, E. Larson, C. J. Carey, İ. Polat, Y. Feng, E. W. Moore, J. VanderPlas, D. Laxalde, J. Perktold, R. Cimrman, I. Henriksen, E. A. Quintero, C. R. Harris, A. M. Archibald, A. H. Ribeiro, F. Pedregosa, P. van Mulbregt, SciPy 1.0 Contributors, SciPy 1.0: Fundamental algorithms for scientific computing in Python. *Nat. Methods* **17**, 261–272 (2020).

Acknowledgments

Funding: This research was supported by the Pioneer Research Center Program through the National Research Foundation of Korea funded by the Ministry of Science, ICT & Future Planning (RS-2022-NR067569) (to Y.C.); the Bio&Medical Technology Development Program of the NRF funded by the Korean government (MSIT) (RS-2024-00440370) (to Y.C.); Basic Science Research Program through the National Research Foundation of Korea (NRF) funded by the Ministry of Education (RS-2024-00410005) (to Y.C.); and KAIST Quantum+X Convergence R&D Project (N10250149) (to S.S.Y.). **Author contributions:** Conceptualization: J.S., T.K., and Y.C. Methodology: J.S., T.K., W.K., and Y.C. Investigation: J.S., T.K., H.C., and Y.C. Formal analysis: J.S., T.K., W.K., and Y.C. Data curation: J.S. and Y.C. Validation: J.S., T.K., and Y.C. Software: W.K. Visualization: T.K., W.K., and Y.C. Resources: S.S.Y. and Y.C. Funding acquisition: S.S.Y. and Y.C. Project administration: T.K. and Y.C. Supervision: Y.C. Writing—original draft: J.S., T.K., and Y.C. Writing—review and editing: J.S., T.K., W.K., S.J., E.C., S.K., H.C., S.S.Y., and Y.C. **Competing interests:** The authors declare that they have no competing interests. **Data, code, and materials availability:** All data and code needed to evaluate and reproduce the results in the paper are present in the paper and/or the Supplementary Materials. This study did not generate new materials. The code used for processing the fluorescence data can be accessed on the following link: https://doi.org/10.5281/zenodo.17520249.

Submitted 3 August 2025
Accepted 4 March 2026
Published 1 April 2026
10.1126/sciadv.aeb1699

Science Advances

Reset-free DNA logic circuits for real-time input processing and memory

Junho Sim, Taehoon Kim, Woojin Kim, Sangeun Jeong, Eunjin Choi, Sion Kim, Hansol Choi, Sung Sun Yim, and Yeongjae Choi

Sci. Adv. **12** (14), eaeb1699. DOI: 10.1126/sciadv.aeb1699

Science Advances (ISSN 2375-2548) is published by the American Association for the Advancement of Science. 1200 New York Avenue NW, Washington, DC 20005. The title *Science Advances* is a registered trademark of AAAS.